

# Topological Anderson insulators with different bulk states in quasiperiodic chains

Ling-Zhi Tang,<sup>1</sup> Shu-Na Liu,<sup>1</sup> Guo-Qing Zhang,<sup>1,2</sup> and Dan-Wei Zhang<sup>1,2,\*</sup>

<sup>1</sup>*Guangdong Provincial Key Laboratory of Quantum Engineering and Quantum Materials,  
School of Physics and Telecommunication Engineering,  
South China Normal University, Guangzhou 510006, China*

<sup>2</sup>*Guangdong-Hong Kong Joint Laboratory of Quantum Matter,  
Frontier Research Institute for Physics, South China Normal University, Guangzhou 510006, China*

(Dated: January 20, 2022)

We investigate the topology and localization of one-dimensional Hermitian and non-Hermitian Su-Schrieffer-Heeger chains with quasiperiodic hopping modulations. In the Hermitian case, phase diagrams are obtained by numerically and analytically calculating various topological and localization characters. We show the presence of topological extended, intermediate, and localized phases due to the coexistence of topological and localization phase transitions driven by the quasiperiodic disorder. In particular, we uncover three types of disorder-induced topological Anderson insulators (TAIs) with extended, intermediate, and localized bulk states in this chiral chain. Moreover, we study the non-Hermitian effects on the TAIs by considering two kinds of non-Hermiticities from the non-conjugate complex hopping phase and asymmetric hopping strength, respectively. We demonstrate that three types of TAIs preserve under the non-Hermitian perturbations with some unique localization and topological properties, such as the non-Hermitian real-complex and localization transitions and their topological nature.

## I. INTRODUCTION

Topological insulators, hosting topological invariants for bulk states and nontrivial in-gap edge modes, have been widely explored in condensed matter [1, 2] and artificial systems [3–13]. Due to the global topology of band structures, topological insulators are immune to weak disorder or local perturbations. However, strong disorders usually drive the systems into trivial gapless insulators as all the bulk states becomes Anderson localized [14]. Unexpectedly, it was theoretically found that a topological phase transition from trivial phases to topological insulators with robust edge states can be driven by moderate disorders [15]. Such a disorder-induced topological phase is dubbed as topological Anderson insulators (TAIs). Actually, the underlying mechanism of TAIs is the renormalization of topological terms by disorders [15–17], instead of the disorder-induced localization phenomenon.

In recent years, the TAIs and their generalizations have been revealed in various systems [15–30], even in some non-Hermitian systems [31–37] and in the presence of inter-particle interactions [38–40]. Some of them have been experimentally observed in engineered lattices, such as cold atomic gases [41], photonic and sonic crystals [42–44], electric circuits [45], and photonic quantum walks [36]. However, the interplay between disorder-induced topological and localization transitions remains largely unexplored. In particular, in most of these work, random disorders are considered and thus bulk states of the TAIs are fully localized, such as in one-dimensional (1D) Su-Schrieffer-Heeger (SSH) model [46] with random hopping strengths [19, 20, 41].

Quasiperiodic systems with incommensurate modulations in the potential or hopping terms are an ideal platform to study the Anderson localization and topological phases of matter [47–68]. The quasiperiodic disorder can lead to localization phenomena without counterparts of random disorder in low dimensions, such as the localization transition [47–50], the intermediate phase consisting of both localized and extended states [51, 69–74], and the critical phase consisting of only critically localized states [67, 75–79]. Meanwhile, the topological charge pumping [49] can be realized in the paradigmatic 1D Aubry-André-Harper model [47, 48] and its variety of generalizations [53–60]. Very recently, the topological phase with critically localized bulk states in a quasiperiodic lattice [67] and the (non-quantized) pumping induced by the quasiperiodic disorder [68] were experimentally observed with cold atoms. However, it remains unclear whether the quasiperiodic disorder can induce TAIs with different localization properties of bulk states.

On the other hand, growing effort has recently been made to explore topological and localization physics in non-Hermitian Hamiltonians or systems [80–90]. For instance, in the presence of non-Hermiticities from non-reciprocal hopping [63, 91–94] or complex on-site potential [69, 93–97], it has been revealed that topological phase transition characterized by a spectral winding number coincides with localization transition and (or) real-complex transition [63, 69, 79, 97, 98]. The non-Hermitian quasiperiodic systems may exhibit generalized mobility edge [93, 96]. Moreover, exotic non-Hermitian TAIs induced by non-reciprocal hopping terms with random disorders in the generalized SSH model has been proposed and observed in Refs. [31–36]. It would be interesting to further study the disorder-induced TAIs in non-Hermitian quasiperiodic systems.

In this work, we explore the interplay of topology and

\* danweizhang@m.scnu.edu.cn

localization in Hermitian and non-Hermitian SSH chains with quasiperiodic hopping disorders. In the Hermitian case, we obtain the phase diagrams by numerically calculating various topological and localization properties. The numerical results consist with the analysis of topological boundaries obtained from the localization length of zero modes and the self-consistent Born approximation (SCBA). We show the topological extended, intermediate (partially localized), and localized phases due to the coexistence of topological and localization phase transitions driven by the quasiperiodic disorder. In particular, we uncover three types of disorder-induced TAIs with extended, intermediate, and localized bulk states in this system. Moreover, we study the non-Hermitian effects on the TAIs by considering two kinds of non-Hermiticities from the non-conjugate complex hopping phase and asymmetric hopping strength, respectively. We find that the proposed three types of TAIs preserve under the non-Hermitian perturbations. We also reveal some unique localization and topological properties in these two cases, such as the non-Hermitian real-complex and localization transitions and their topological nature.

The rest of the paper are organized as follow. We first reveal three types of TAIs in the Hermitian SSH chain with the quasiperiodic hopping modulation in Sec. II. Section III is then devoted to investigate non-Hermitian effects on the topological and localization properties of the uncovered TAIs. A brief conclusion is presented in Sec. IV.

## II. TAIS WITH DIFFERENT BULK STATES

We start by considering a generalized SSH model in a 1D dimerized lattice (denoted by  $A$  and  $B$  sublattices) with quasiperiodic disordered hopping. The system is described by the following tight-binding Hamiltonian

$$H = \sum_{n=1}^N (m_n a_n^\dagger b_n + t a_{n+1}^\dagger b_n + \text{H.c.}), \quad (1)$$

where  $N$  is the number of unit cell,  $a_n^\dagger$  ( $b_n$ ) denotes the creation (annihilation) operator for a particle on the  $A$  ( $B$ ) sublattice of the  $n$ -th cell, and  $t$  and  $m_n$  is the constant inter-cell hopping strength and the site-dependent intra-cell hopping strength, respectively. In this Hermitian system ( $H = H^\dagger$ ), we consider the quasiperiodic modulation on the intra-cell hopping term as

$$m_n = m + W \cos(2\pi\alpha n), \quad (2)$$

where  $m$  is an overall intra-cell hopping strength,  $W$  denotes the quasiperiodic disorder, and  $\alpha$  is chosen as an irrational number to ensure the incommensurate modulation. In the clean limit with  $W = 0$ , the Hamiltonian in Eq. (1) reduces to the original SSH model with topological (trivial) phase when  $m < t$  ( $m > t$ ), which is characterized by the 1D winding number and protected by the chiral symmetry.

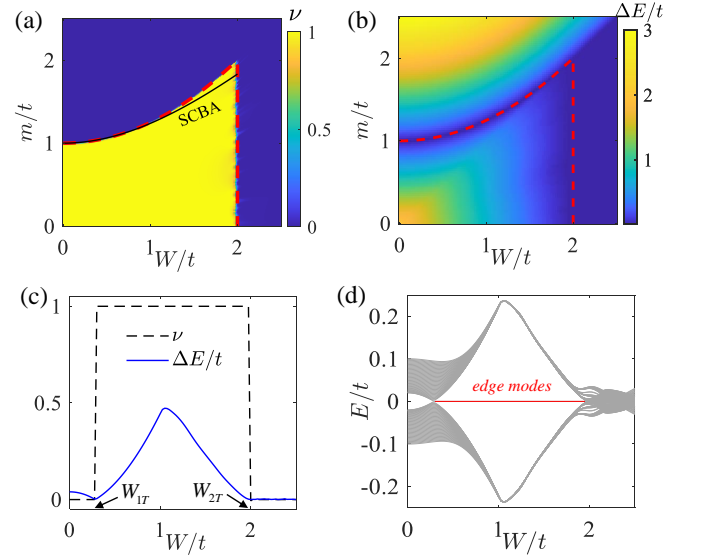


FIG. 1. (Color online) (a) Real-space winding number  $\nu$ , (b) energy gap  $\Delta E$  as functions of  $W$  and  $m$ . The red dash and black solid lines denote the topological phase boundaries determined by the divergence of the localization length of zero-energy states and from the SCBA analysis, respectively. (c)  $\nu$  (red dash line) and  $\Delta E$  (blue solid line) as a function of  $W$  for  $m = 1.02$  with  $W_{1T}$  and  $W_{2T}$  being the topological transition points. (d) The middle 100 eigenenergies as a function of  $W$  for  $m = 1.02$  under OBCs, with two zero-energy edge modes when  $W_{1T} < W < W_{2T}$  colored in red.

In the following, we investigate the topology and localization in the model with the quasiperiodic hopping disorder, which still preserves the chiral symmetry. We set  $t = 1$  as the energy unit,  $\alpha = (\sqrt{5} - 1)/2$  as the golden ratio, and the lattice size  $N = 610$  in our numerical simulations. The periodic boundary conditions (PBCs) is considered unless mentioned otherwise.

### A. Topological phase diagram and transitions

To characterize the topological properties of the disordered chiral chain that breaks the translation symmetry, we use the real-space winding number defined by [20]

$$\nu = \frac{1}{L'} \text{Tr}'(\Gamma Q[Q, X]). \quad (3)$$

Here  $Q = \sum_{j=1}^N (|j\rangle \langle j| - |\tilde{j}\rangle \langle \tilde{j}|)$  is obtained by solving the equation  $H|\tilde{j}\rangle = E_j|\tilde{j}\rangle$  and  $|\tilde{j}\rangle = \Gamma^{-1}|j\rangle$  with eigenenergies  $E_j$  and eigenstates  $|j\rangle$ ,  $\Gamma = I_N \otimes \sigma_z$  is the chiral symmetry operator with the identity matrix  $I_N$  and the Pauli matrix  $\sigma_z$ ,  $X$  is the coordinate operator, and  $\text{Tr}'$  denotes the trace over the middle interval of the lattice with the length  $L' = L/2$ .

The topological phase diagram on the  $W$ - $m$  plane obtained by numerically computing  $\nu$  is shown in Fig. 1(a). In the clean limit  $W = 0$ , the topological transition between the trivial phase with  $\nu = 0$  and the topological

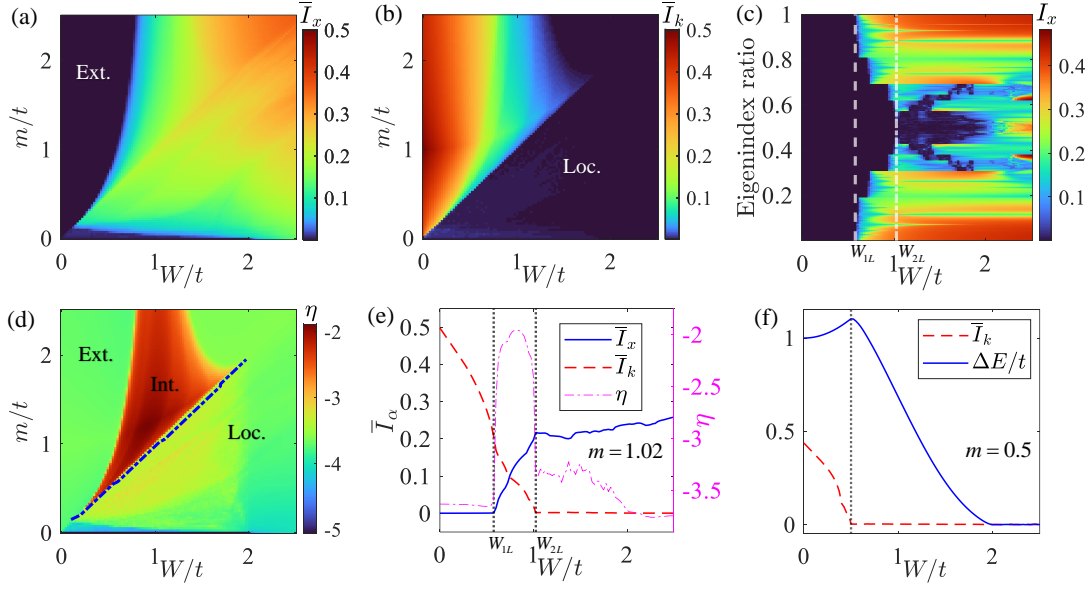


FIG. 2. (Color online) Averaged IPRs  $\bar{I}_x$  (a) and  $\bar{I}_k$  (b) and quantity  $\eta$  (d) on the parameter space  $W$ - $m$ . (c) The IPR  $I_x$  associated to eigenstates as a function of  $W$  for fixed  $m = 1.02$ . (e)  $\bar{I}_x$  (blue solid line),  $\bar{I}_k$  (red dash line) and bulk gap  $\Delta E$  (blue solid line) as a function of  $W$  for  $m = 0.5$ . In (a,b,d), the regions for extended, localized and intermediate phases are denoted by 'Ext.', 'Loc.' and 'Int.', respectively. In (c,e), the vertical lines with  $W_{1L} \approx 0.57$  and  $W_{2L} \approx 1.02$  denote the first and second localization transitions, respectively. The blue dash-dot line in (d) denotes the inflection point of  $\Delta E$  with varying  $W$ .

phase with  $\nu = 1$  occurs at  $m = 1$ . The topological region for the constant intra-cell hopping strength  $m$  enlarges when increasing  $W$  to a modest regime. One can find the TAIs driven by the quasiperiodic disorder from the trivial phase when  $1 < m \lesssim 2$ . The disorder-induced TAI regime is similar to that in the SSH model with random hopping disorders [19, 20, 41], however, it contains three different kinds of bulk states as we will discuss below.

We also compute the bulk gap  $\Delta E = E_{N+1} - E_N$  under the PBCs, as shown in Fig. 1(b). The bulk gap closes at the topological transition points and becomes vanishing for trivial gapless Anderson insulators when  $W$  is large enough ( $W \gtrsim 2$ ). To be more clear, we plot  $\nu$  and  $\Delta E$  as a function of  $W$  for fixed  $m = 1.02$  in Fig. 1(c). One can find the disorder-induced TAIs lying between the first and second topological transition points at  $W_{1T} \approx 0.27$  and  $W_{2T} \approx 2.0$ , respectively. The disorder-induced zero-energy edge modes in the energy spectrum of the TAIs phase under the open boundary conditions (OBCs) are shown in Fig. 1(d), owing to the bulk-boundary correspondence.

At the topological transition points, the localization length of zero-energy modes are divergent due to their delocalization nature in 1D chiral chains [20]. For our model Hamiltonian, the wave function of zero-energy eigenstate  $\psi = \{\psi_{1,A}, \psi_{1,B}, \psi_{2,A}, \psi_{2,B} \cdots \psi_{N,A}, \psi_{N,B}\}^T$  can be obtained by solving the corresponding Schrödinger equation  $H\psi = 0$ . This corresponds to the eigen-equations  $t\psi_{n,B} + m_n\psi_{n+1,B} = 0$  and  $m_n\psi_{n,A} + t\psi_{n+1,A} = 0$ , which

leads to the form of the probability distribution of the zero-energy wave function

$$\begin{aligned} \psi_{n,A} &= (-1)^n \prod_{l=1}^n \frac{m_l}{t} \psi_{1,A}, \\ \psi_{n,B} &= (-1)^n \prod_{l=1}^n \frac{t}{m_{l+1}} \psi_{1,B}. \end{aligned} \quad (4)$$

Thus, the inverse of localization length ( $\Lambda$ ) of zero-energy modes in the limit  $N \rightarrow \infty$  reads

$$\Lambda^{-1} = \max \left\{ \lim_{N \rightarrow \infty} \frac{1}{N} \ln |\psi_{N,A}|, \lim_{N \rightarrow \infty} \frac{1}{N} \ln |\psi_{N,B}| \right\}. \quad (5)$$

By setting  $\psi_{1,A} = \psi_{1,B} = 1$ , one can obtain

$$\begin{aligned} \lim_{N \rightarrow \infty} \frac{1}{N} \ln |\psi_{N,A}| &= \lim_{N \rightarrow \infty} \frac{1}{N} \ln |\psi_{N,B}| \\ &= \lim_{N \rightarrow \infty} \frac{1}{N} \sum_{l=1}^N (\ln |t| - \ln |m_l|). \end{aligned} \quad (6)$$

Substituting Eq. (5) into Eq. (6), we obtain

$$\Lambda^{-1} = \lim_{N \rightarrow \infty} \frac{1}{N} \sum_{l=1}^N (\ln |t| - \ln |m_l|). \quad (7)$$

Note that  $\Lambda^{-1} \rightarrow 0$  when the localization length diverges ( $\Lambda \rightarrow \infty$ ). We show the results of  $\Lambda^{-1} \approx 0$  [numerically obtained by solving Eq. (7)] as the red dash lines in Figs.

1(a) and 1(b). The results indicate that topological and trivial phases can be well separated by the delocalization nature of zero modes in this quasiperiodic system.

We further perform the SCBA analysis to reveal the disorder-induced renormalization of the topological term for the TAIs in the topological phase diagram [Fig. 1(a)]. This analysis works in the region  $W \lesssim 2$  where the disorder is not dominated. Based on the effective medium theory and the SCBA method [16], one can self-consistently obtain the disorder-induced self-energy as the renormalization of a clean Hamiltonian. For the Hamiltonian in Eq. (1), the self-energy term  $\Sigma(W)$  satisfies the self-consistent equation

$$\frac{1}{E_F - H_q(k) - \Sigma(W)} = \langle \frac{1}{E_F - H_{\text{eff}}(k, W)} \rangle, \quad (8)$$

where  $E_F \equiv 0$  is Fermi energy,  $H_q(k) = [m + t \cos(k)]\sigma_x + t \sin(k)\sigma_y$  is the clean Hamiltonian ( $W = 0$ ) in momentum space with  $\sigma_{x,y}$  the Pauli matrices,  $\Sigma = \Sigma_x \sigma_x + \Sigma_y \sigma_y$  and the  $\langle \dots \rangle$  denotes averaging over all disorder samples. In our model, the quasiperiodic disorder follows the form  $V(n)\sigma_x$  with  $V(n) = W \cos(2\pi\alpha n)$ , thus the effective Hamiltonian  $H_{\text{eff}} = H_q(k) + V(n)\sigma_x$ . Considering the symmetry of the Hamiltonian, the self-energy is simplified as  $\Sigma(W) = \Sigma_x(W)\sigma_x$ . The intra-cell hopping strength  $m$  is then renormalized as  $\bar{m} = m + \Sigma_x(W)$ . The topological phase boundary on the  $m$ - $W$  plane is determined by  $\bar{m}(m, W) = t$ . The numerical results of the topological phase boundary based on the SCBA for small and modest disorder strength is shown as the black solid line in Fig. 1(a), which agree well with that determined by the winding number.

### B. Localization properties of bulk states

We now study the localization properties of bulk states in this model. To do this, we first numerically compute the inverse participation ratio (IPR) of the  $j$ -th eigenstate in real and momentum spaces [99]

$$I_\beta(j) = \sum_{\beta} |\langle \beta | j \rangle|^4, \quad (9)$$

where the wave function  $|j\rangle$  is normalized to unity and  $\beta = x, k$  denotes the basis in real and momentum spaces, respectively. For large lattice size  $L = 2N$  in our model,  $I_x \sim \mathcal{O}(1)$  and  $I_k \sim \mathcal{O}(L^{-1})$  indicate a localized eigenstate, while  $I_x \sim \mathcal{O}(L^{-1})$  and  $I_k \sim \mathcal{O}(1)$  for an extended eigenstate. The localization of the overall bulk states can be characterized by the averaged IPR over the whole energy spectrum

$$\bar{I}_\beta = \frac{1}{L} \sum_{j=1}^L I_\beta(j). \quad (10)$$

Figures 2(a) and 2(b) show the numerical results of  $\bar{I}_x$  and  $\bar{I}_k$  on the  $W$ - $m$  plane, respectively. We can find the

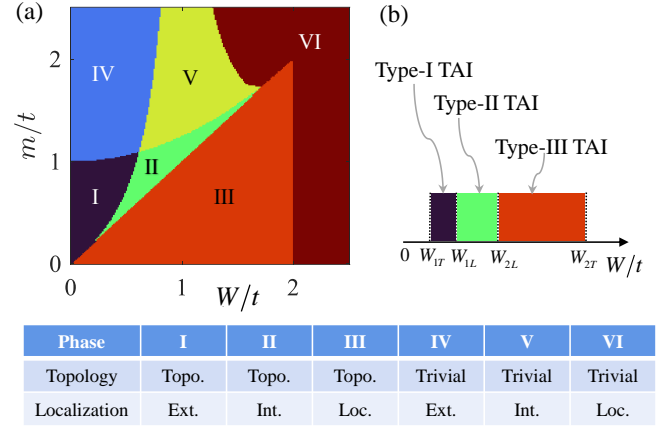


FIG. 3. (Color online) (a) Phase diagram on the  $W$ - $m$  parameter space. There are six different phases: extended topological phase (I), topological intermediate phase (II), topological localized phase (III), trivial extended phase (IV), trivial intermediate phase (V), and trivial localized phase (VI), as illustrated in the table. (b) Regions of  $W$  with fixed  $m = 1.02$  for three types of TAIs induced by the quasiperiodic disorder.

extended (localized) phase consisting of fully extended (localized) eigenstates with  $\bar{I}_x \rightarrow 0$  ( $\bar{I}_k \rightarrow 0$ ). However, there is an intermediate region with  $\bar{I}_\beta \neq 0$  lying between the extended and localized phases on the  $W$ - $m$  plane. To figure out the localization properties in this regime, we display  $I_x$  as a function of  $W$  with respect to all eigenstates for  $m = 1.02$  in Fig. 2(c). One can see that such an intermediate phase is partially localized (with the mobility edge) and consists of both extended and localized eigenstates lying between the first and second localization transition points at  $W = W_{1L} \approx 0.57$  and  $W = W_{2L} \approx 1.02$  [also see Fig. 2(e)], respectively.

To further characterize the intermediate phase, we can use the dimensional parameter

$$\eta = \log_{10}(\bar{I}_x \times \bar{I}_k). \quad (11)$$

Figure 2(d) displays the numerical results of  $\eta$  on the  $W$ - $m$  plane, where the parameter region for the intermediate phase with relatively large  $\eta$  is clearly shown. We also plot  $\bar{I}_{x,k}$  and  $\eta$  as a function of  $W$  with fixed  $m = 1.02$  in Fig. 2(e). In the extended phase when  $0 \leq W < W_{1L}$  and the localized phase when  $W > W_{2L}$  with  $W_{1L} \approx 0.57$  and  $W_{2L} \approx 1.02$ , one has vanishing  $\bar{I}_x$  and  $\bar{I}_k$ , respectively. In the intermediate phase when  $W_{1L} < W < W_{2L}$ , both of  $\bar{I}_x$  and  $\bar{I}_k$  are finite with a relatively large value of  $\eta$ . In addition, we numerically find that the inflection points of the energy gap  $\Delta E$  with varying  $W$  nearly coincide with the transition points from the intermediate phase to the localized phase, which are denoted by the blue dash line in Fig. 2(d). To see the coincidence, in Fig. 2(f), we plot  $\Delta E$  and  $\bar{I}_k$  with varying  $W$  for  $m = 0.5$  as an example.

Combining the topological and localization phase diagrams in Figs. 1(a) and 2(d), we finally obtain the total phase diagram on the  $W$ - $m$  plane, as shown in Fig.

3(a). There are six phases in the phase diagram determined by different topological and localization properties. They are labeled from I to VI: Phases I, II and III are topological with extended, intermediate, localized bulk states, respectively; and Phases IV, V and VI are trivial with extended, intermediate, localized bulk states, respectively. Thus, we obtain three types of TAIs with different localization properties of bulk states. For instance, as shown in Fig. 3(b) with  $m = 1.02$ , one can find the disorder-driven transition from trivial extended phase to the TAIs with extended ( $W_{1T} < W < W_{1L}$ ), intermediate ( $W_{1L} < W < W_{2L}$ ) and localized bulk states ( $W_{2L} < W < W_{2T}$ ), which are dubbed as type-I, type-II and type-III TAIs, respectively. For strong disorder ( $W > W_{2T}$ ), the system becomes trivial gapless phase with fully localized states. Notably, the quasiperiodic disorder induced TAIs with extended and intermediate bulk states uncovered here are absent in random disordered systems. For instance, only the (type-III) TAI with fully localized bulk states exhibits in the SSH model with random disorder hopping [19, 20, 41].

### III. NON-HERMITIAN TAIS

In this section, we proceed to study the non-Hermitian effects on the three types of TAIs. In Sec. III A, we consider the non-Hermiticity induced by non-conjugate complex hopping phase. We also consider the asymmetric hopping strength in Sec. III B. We find that three types of TAIs preserve and exhibit some properties unique to the non-Hermitian systems.

#### A. Non-conjugate hopping-phase case

We introduce the non-Hermiticity to the hopping term of the model Hamiltonian in Eq. (1), which now becomes

$$H' = \sum_{n=1}^N m'_n a_n^\dagger b_n + m'_n b_n^\dagger a_n + (t a_{n+1}^\dagger b_n + \text{H.c.}), \quad (12)$$

with the modified intra-cell hopping term

$$m'_n = m + W \cos(2\pi\alpha n + ih). \quad (13)$$

Here the non-Hermiticity parameter is the complex phase  $h$  [100], which leads to the non-conjugate hopping ( $m'_n \neq m'^*_n$ ) without breaking the chiral symmetry.

As shown in Refs. [31, 32, 101], the real-space winding number  $\nu$  can be generalized to non-Hermitian Hamiltonians under the biorthogonal basis. To this end, the matrix  $Q$  in Eq. (3) is replaced by  $Q = \sum_{j=1}^N (|j'R\rangle \langle j'L|) - |\tilde{j}'R\rangle \langle \tilde{j}'L|$ . Here right eigenstates  $|j'R\rangle$  and left eigenstates  $|\tilde{j}'L\rangle$  are obtained from the eigenfunctions  $H'|j'R\rangle = E_{j'R}|j'R\rangle$  and  $H^\dagger|\tilde{j}'L\rangle = E_{\tilde{j}'L}|\tilde{j}'L\rangle$  with  $|\tilde{j}'R\rangle = \Gamma^{-1}|j'R\rangle$  and  $|\tilde{j}'L\rangle = \Gamma^{-1}|j'L\rangle$ ,

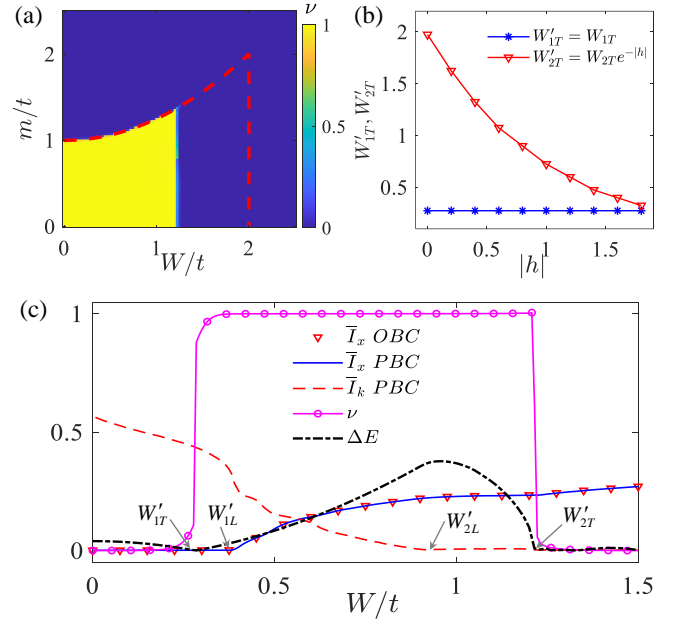


FIG. 4. (Color online) (a)  $\nu$  as functions of  $W$  and  $m$  for  $h = 0.5$ . Red dash line denoted the topological phase boundary in the Hermitian case ( $h = 0$ ). (b) The first and second topological transition points  $W'_{1T}$  and  $W'_{2T}$  for varying non-Hermiticity parameter  $|h|$  and fixed  $m = 1.02$ . (c)  $\nu$ ,  $\bar{I}_{x,k}$  (under the PBCs and OBCs), and  $\Delta E$  as a function of  $W$  for  $m = 1.02$  and  $h = 0.5$ . The two topological and localization transition points at  $W'_{1T} \approx 0.27$ ,  $W'_{2T} \approx 1.21$ ,  $W'_{1L} \approx 0.39$ , and  $W'_{2L} \approx 0.92$  are labeled.

which form the biorthogonal basis. We numerically calculate  $\nu$  on the  $W$ - $m$  plane for  $h = 0.5$ , as shown in Fig. 4(a), where the red dash line denotes the topological phase boundary in the Hermitian case [ $h = 0$  in Fig. 1(a)]. One can find that this kind of non-Hermiticity with finite  $|h|$  reduces the topological region by moving the second topological transition from  $W_{2T}$  to  $W'_{2T} < W_{2T}$ , while keeps the first topological transition at  $W'_{1T} = W_{1T} < W'_{2T}$ . To be more clearly, we plot the  $W'_{1T}$  and  $W'_{2T}$  as a function of  $|h|$  for  $m = 1.02$  in Fig. 4(b). They are well fitting by  $W'_{1T} = W_{1T}$  and  $W'_{2T} = W_{2T}e^{-|h|}$ , with  $W_{1T} \approx 0.27$  and  $W_{2T} \approx 2.0$  in the Hermitian limit.

In Fig. 4(c), we plot the winding number  $\nu$  and the energy gap  $\Delta E = \text{Re}(E_{N+1,R} - E_{N,R})$  defined by the real part of the complex eigenenergies  $E_{N,R}$  (sorted by the real part of spectrum) as a function of  $W$  for  $m = 1.02$  and  $h = 0.5$ . The two topological phase transitions happen at  $W'_{1T} \approx 0.27$  and  $W'_{2T} \approx 1.21$  with the gap closing. To reveal the localization properties in this non-Hermitian case, we calculate the IPRs  $\bar{I}_{x,k}$  averaged over the right eigenstates  $|j'R\rangle$ . The results of  $\bar{I}_x$  are the same under PBCs and OBCs in both the clean and disordered cases. This indicates the absence of non-Hermitian skin effect [85–90] of bulk states under OBCs. With the results of  $\bar{I}_\beta$ , we can obtain the first and second localiza-

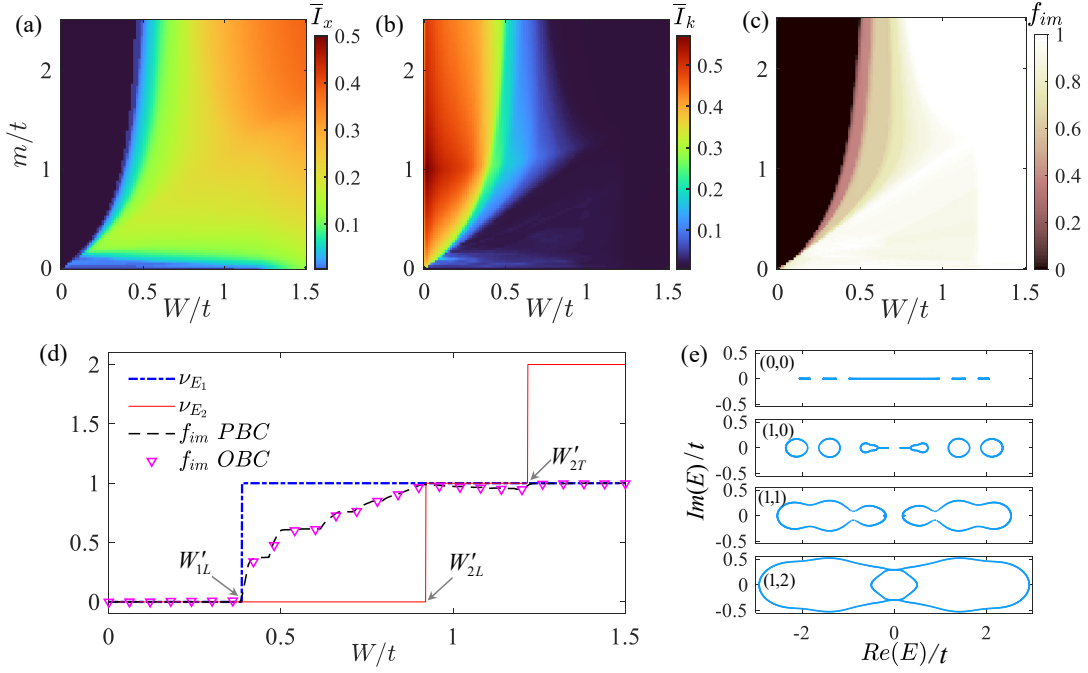


FIG. 5. (Color online) Averaged IPR  $\bar{I}_x$  (a) and  $\bar{I}_k$  (b) and ratio of complex eigenenergies  $f_{im}$  (c) under PBCs for  $h = 0.5$  on the parameter space  $W$ - $m$ . (d) Plot of spectral winding number  $\nu_{E_1}$  (blue dash line),  $\nu_{E_2}$  (red dash line),  $f_{im}$  for PBCs (black dash line) and  $f_{im}$  for OBCs (pink inverted triangle) for  $m = 1.02$ ,  $h = 0.5$  as a function of  $W$ . The two localization transition points  $W'_{1L} \approx 0.39$  and  $W'_{2L} \approx 0.92$ , and the topological transition point  $W'_{2T} \approx 1.21$  are labeled. (e) Typical energy spectrum for  $W = 0.3, 0.8, 1, 1.4$  (from top to bottom) with the energy winding numbers ( $\nu_{E_1}, \nu_{E_2}$ ) in each panel for  $h = 0.5$ .

tion transition points at  $W'_{1L} \approx 0.39$  and  $W'_{2L} \approx 0.92$ . Thus, the three types of TAIs can still be induced by the quasiperiodic disorder in this non-Hermitian system when  $0.27 \lesssim W \lesssim 0.39$  (type-I),  $0.39 \lesssim W \lesssim 0.92$  (type-II), and  $0.92 \lesssim W \lesssim 1.21$  (type-III), respectively. In Figs. 5(a) and 5(b), we further show the results of  $\bar{I}_{x,k}$  under PBCs on the  $W$ - $m$  plane with  $h = 0.5$ . Comparing to the results for  $h = 0$  in Figs. 2(a) and 2(b), we can find that the non-Hermiticity enlarges the parameter region of the localized phase and reduces the extended and intermediate phase regions. The result indicates that the non-conjugate hopping tends to localize the bulk states.

The real-complex transition of the energy spectrum and its winding on the complex energy plane are unique to non-Hermitian Hamiltonians [80–82]. To study the real-complex transition, we numerically compute the ratio of the right eigenstates  $|jR\rangle$  with complex eigenenergies in the energy spectrum, which is defined by

$$f_{im} = L_{im}/L, \quad (14)$$

with  $L_{im}$  the number of eigenenergies whose imaginary part  $|\text{Im}(E_{jR})| > 10^{-13}$  as the cutoff in our simulations. The numerical result of  $f_{im}$  for  $h = 0.5$  on the  $W$ - $m$  plane is shown in Fig. 5(c). We find that the energy spectrum is either real ( $f_{im} = 0$ ) or complex ( $0 < f_{im} \leq 1$ ) in the phase diagram. The boundary between the real and complex energies corresponds to the localization-delocalization phase boundary in Fig. 5(a). To see the coincidence more clearly, we plot  $f_{im}$  under PBCs and

OBCs as a function of  $W$  in Fig. 5(d), with the localization transition points  $W'_{1L}$  and  $W'_{2L}$  being labeled. One can see that  $f_{im}$  turns to non-zero at  $W'_{1L}$ , which shows that the real-complex transition coincides with the localization transition from the extended to intermediate phases. In addition,  $f_{im} \approx 1$  in the fully localized phase when  $W \gtrsim W'_{2L}$ . Here the independence of  $f_{im}$  on the boundary condition also indicates the absence of the non-Hermitian skin effect in this case with the non-conjugate hopping phase.

To characterize the topology of the energy spectrum in this non-Hermitian quasiperiodic chain, we can use the spectral winding numbers defined as [83]

$$\nu_\mu = \int_0^{2\pi} \frac{d\theta}{2\pi i} \partial_\theta \ln \det [\mathcal{H}(\theta) - \mu]. \quad (15)$$

Here the modified Hamiltonian  $\mathcal{H}(\theta) = H'(\theta)$  with respect to the additional periodic modulation phase  $\theta$  is given by rewriting  $m'_n$  in Eq. (12) as

$$m'_n(\theta) = m + W \cos(2\pi\alpha n + i h + \theta). \quad (16)$$

In addition, the indexes  $\mu = E_1, E_2$  denote the real parts of eigenenergies for the eigenstates with the smallest and maximum IPRs  $I_x$  (for the most extended and localized eigenstates), respectively. Unlike the chiral winding number  $\nu$  for eigenstates, here  $\nu_\mu$  counts how many times the eigenenergy trails enclosing the energy base  $\mu$  on the complex plane when  $\theta$  changes from 0 to  $2\pi$ . Thus,  $\nu_\mu$

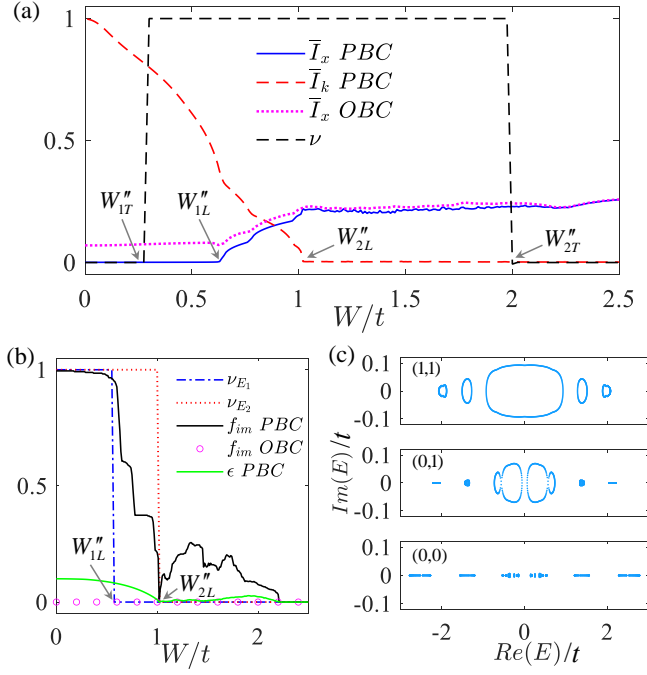


FIG. 6. (Color online) (a)  $\bar{I}_{x,k}$  (under the PBCs and OBCs) and  $\nu$  as a function of  $W$ . Two topological transition points at  $W''_{1T} \approx 0.27$  and  $W''_{2T} \approx 2.0$ , and two localization transition points  $W''_{1L} \approx 0.63$  and  $W''_{2L} \approx 1.02$  are labeled. (b)  $\nu_{E_1}$  (blue dash-dot line),  $\nu_{E_2}$  (red dot line),  $f_{im}$  under PBCs (black solid line),  $f_{im}$  under OBCs (pink round), maximum imaginary part of the energy spectrum  $\epsilon$  (green solid line) as a function of  $W$ . (c) Energy spectrum for  $W = 0.4, 0.7, 1.4$  (from top to bottom) with corresponding  $(\nu_{E_1}, \nu_{E_2})$  inside each panel. Other parameters are  $m = 1.02$  and  $g = 0.1$ .

characterizes the topological structure of the complex energy spectrum, instead of the number of edge modes.

The numerical result of  $\nu_\mu$  for  $h = 0.5$  as a function of  $W$  is shown in Fig. 5(d). We find that the values of  $\nu_{E_1}$  and  $\nu_{E_2}$  change at  $W'_{1L}$  and  $W'_{2T}$ , respectively. In this non-Hermitian chain, the extended and intermediate phases can be characterized by  $(\nu_{E_1}, \nu_{E_2}) = (0, 0)$  and  $(1, 0)$  respectively, while the localized phase takes  $(\nu_{E_1}, \nu_{E_2}) = (1, 1)$  or  $(1, 2)$ . This correspondence can be understood in the assistance of the eigenenergies spectrum shown in Fig. 5(e), with the disorder strength  $W = 0.3, 0.8, 1, 1.4$  (from the top to the bottom panel) for four typical cases. When  $W < W'_{1L}$  with  $W = 0.3$ ,  $\nu_{E_1} = \nu_{E_2} = 0$  due to the real spectrum with  $f_{im} = 0$ . When  $W'_{1L} < W < W'_{2L}$  with  $W = 0.8$ , part of eigenstates become localized with complex eigenenergies that encloses  $E_1$  on the complex plane and thus  $\nu_{E_1} = 1$ . When  $W'_{2L} < W < W'_{2T}$  with  $W = 1$ , most eigenenergies become complex with  $f_{im} \approx 1$  and enclose  $E_{1,2}$  with  $\nu_{E_1} = \nu_{E_2} = 1$ . Interestingly, we find that the transition from  $\nu_{E_2} = 1$  to  $\nu_{E_2} = 2$  coincides with that from  $\nu = 1$  to  $\nu = 0$  at  $W'_{2T}$ , due to the band crossing at this topological transition point. These results demonstrate the coincidence of disorder-induced real-complex,

localization and topological transitions, as well as the existence of the three types of TAIs in this non-Hermitian quasiperiodic lattice.

## B. Asymmetric hopping-strength case

We consider another kind of non-Hermiticity induced by the asymmetric hopping strength [85–92] in our model, which reads

$$H'' = \sum_{n=1}^N (m_n a_n^\dagger b_n + \text{H.c.}) + t e^{-g} a_{n+1}^\dagger b_n + t e^g b_n^\dagger a_{n+1}. \quad (17)$$

Here  $g$  denotes the asymmetric parameter. Notably, in this case  $\mathcal{H}(\theta) = H''(\theta)$  in Eq. (15), with  $H''(\theta)$  defined by adding the periodically twisted phase  $\theta$  to the asymmetric hopping under the PBCs:  $g \rightarrow g - i\theta/L$  in Eq. (17). We plot  $\nu$  as a function of  $W$  for  $m = 1.02$  and  $g = 0.1$  in Fig. 6(a). The disorder-induced topological transitions in this case happen at  $W = W''_{1T} = W_{1T} \approx 0.27$  (from trivial phase to TAIs) and  $W = W''_{2T} = W_{2T} \approx 2.0$  (from TAIs to trivial phase). This can be understood from the fact that  $H''$  can be transformed to  $H$  under OBCs through a similarity transformation  $H = S H'' S^{-1}$  with  $S = \text{diag}\{1, 1, e^{-g}, e^{-g}, e^{-2g}, e^{-2g}, \dots, e^{-Ng}, e^{-Ng}\}$ . The corresponding eigenstates  $|j''\rangle$  can be obtained via  $|j''\rangle = S^{-1} |j\rangle$  with the same real eigenenergies of  $H$ . This leads to the non-Hermitian skin effect for bulk states of  $H''$  under the OBCs.

We calculate  $\bar{I}_{x,k}$  and find the localization transition points  $W''_{1L} \approx 0.63 > W_{1L}$  and  $W''_{2L} = W_{2L} \approx 1.02$  with increasing  $g$  in Fig. 6(a). The asymmetric hopping tends to enlarge (keep) the extend (fully localized) phase region and reduce the intermediate phase region. Notably, the averaged IPR  $\bar{I}_x$  under OBCs is larger than that under PBCs in extended and intermediate phases due to the non-Hermitian skin effect in this case [31]. In the localized phase for  $W > W''_{2L}$ ,  $\bar{I}_x$  takes nearly the same values for OBCs and PBCs as the skin effect of bulk states is destroyed by strong disorders.

In Fig. 6(b), we numerically calculate  $\nu_\mu$ , the imaginary fraction  $f_{im}$  and the maximum imaginary part in the energy spectrum  $\epsilon = \max[\text{Im}(E_j)]$  as a function of  $W$  for  $m = 1.02$  and  $g = 0.1$ . In this asymmetric hopping case, the eigenenergies of  $H''$  under OBCs are the same to those of  $H$ . Thus,  $f_{im} = 0$  for all  $W$  and there is no real-complex transition under OBCs. In addition,  $\nu_{E_1}$  and  $\nu_{E_2}$  change at the localization transition points  $W''_{1L}$  and  $W''_{2L}$ , respectively. However, the disorder-induced real-complex transition under PBCs happens at  $W \approx 2.21 > W''_{2L} > W''_{1L}$ . We also plot the energy spectra for  $W = 0.3, 0.8, 1.4$  in Fig. 6(c). When  $0 \leq W < W''_{1L}$  with  $W = 0.3$ , complex eigenenergies enclose  $E_1$  and  $E_2$  with  $f_{im} \approx 1$  and  $\nu_{E_1} = \nu_{E_2} = 1$ . Increasing disorder strength when  $W''_{1L} < W < W''_{2L}$  with  $W = 0.8$ , part of eigenenergies become real and thus  $\nu_{E_2} = 0$ . When  $W > W''_{2L}$  with  $W = 1.4$ , most

eigenenergies become real with  $f_{im} \approx 0$  and  $\epsilon \approx 0$ , such that  $\nu_{E_1} = \nu_{E_2} = 0$ . These results demonstrate that the existence of the three types of TAIs under the asymmetric hopping. The disorder-induced localization transition coincides with the real-complex transition under PBCs, but are not related to the topological transition in this case.

#### IV. CONCLUSION

In summary, we have explored the topology and localization of Hermitian and non-Hermitian SSH chains with quasiperiodic hopping disorders. In the Hermitian case, we have obtained the phase diagrams with topological extended, intermediate and localized phases. Due to the coexistence of topological and localization transitions, we have uncovered three types of disorder-induced TAIs with extended, intermediate, and localized bulk states in the system. We have also studied the non-Hermitian effects on the TAIs by considering two kinds of non-Hermiticities from the non-conjugate hopping phase and asymmetric hopping strength, respectively. We have

shown that the three types of TAIs can preserve and exhibit some unique localization and topological properties in these non-Hermitian cases.

*Note added.* After completion of this manuscript, we noticed a very recent work (arXiv:2201.00488) on a similar problem [102], where the TAI with intermediate bulk states and exact mobility edges were obtained in the Hermitian case. In this paper, we furthermore study the non-Hermitian TAIs.

#### ACKNOWLEDGMENTS

This work was supported by the National Natural Science Foundation of China (Grants No. 12174126 and No. 12104166), the Key-Area Research and Development Program of Guangdong Province (Grant No. 2019B030330001), the Science and Technology Program of Guangzhou (Grant No. 2019050001), and the Guangdong Basic and Applied Basic Research Foundation (Grants No. 2021A1515010315 and No. 2020A1515110290).

- 
- [1] X.-L. Qi and S.-C. Zhang, *Rev. Mod. Phys.* **83**, 1057 (2011).
  - [2] M. Z. Hasan and C. L. Kane, *Rev. Mod. Phys.* **82**, 3045 (2010).
  - [3] D.-W. Zhang, Y.-Q. Zhu, Y. X. Zhao, H. Yan, and S.-L. Zhu, *Advances in Physics* **67**, 253 (2018).
  - [4] N. R. Cooper, J. Dalibard, and I. B. Spielman, *Rev. Mod. Phys.* **91**, 015005 (2019).
  - [5] N. Goldman, J. C. Budich, and P. Zoller, *Nat. Phys.* **12**, 639 (2016).
  - [6] M. D. Schroer, M. H. Kolodrubetz, W. F. Kindel, M. Sandberg, J. Gao, M. R. Vissers, D. P. Pappas, A. Polkovnikov, and K. W. Lehnert, *Phys. Rev. Lett.* **113**, 050402 (2014).
  - [7] P. Roushan, C. Neill, Y. Chen, M. Kolodrubetz, C. Quintana, N. Leung, M. Fang, R. Barends, B. Campbell, Z. Chen, B. Chiaro, A. Dunsworth, E. Jeffrey, J. Kelly, A. Megrant, J. Mutus, P. J. J. O'Malley, D. Sank, A. Vainsencher, J. Wenner, T. White, A. Polkovnikov, A. N. Cleland, and J. M. Martinis, *Nature* **515**, 241 (2014).
  - [8] X. Tan, D.-W. Zhang, Q. Liu, G. Xue, H.-F. Yu, Y.-Q. Zhu, H. Yan, S.-L. Zhu, and Y. Yu, *Phys. Rev. Lett.* **120**, 130503 (2018).
  - [9] X. Tan, D.-W. Zhang, Z. Yang, J. Chu, Y.-Q. Zhu, D. Li, X. Yang, S. Song, Z. Han, Z. Li, Y. Dong, H.-F. Yu, H. Yan, S.-L. Zhu, and Y. Yu, *Phys. Rev. Lett.* **122**, 210401 (2019).
  - [10] C. H. Lee, S. Imhof, C. Berger, F. Bayer, J. Brehm, L. W. Molenkamp, T. Kiessling, and R. Thomale, *Communications Physics* **1**, 39 (2018).
  - [11] S. D. Huber, *Nature Physics* **12**, 621 (2016).
  - [12] L. Lu, J. D. Joannopoulos, and M. Soljačić, *Nature Photonics* **8**, 821 (2014).
  - [13] T. Ozawa, H. M. Price, A. Amo, N. Goldman, M. Hafezi, L. Lu, M. C. Rechtsman, D. Schuster, J. Simon, O. Zilberberg, and I. Carusotto, *Rev. Mod. Phys.* **91**, 015006 (2019).
  - [14] P. W. Anderson, *Phys. Rev.* **109**, 1492 (1958).
  - [15] J. Li, R.-L. Chu, J. K. Jain, and S.-Q. Shen, *Phys. Rev. Lett.* **102**, 136806 (2009).
  - [16] C. W. Groth, M. Wimmer, A. R. Akhmerov, J. Tworzydło, and C. W. J. Beenakker, *Phys. Rev. Lett.* **103**, 196805 (2009).
  - [17] H. Jiang, L. Wang, Q.-F. Sun, and X. C. Xie, *Phys. Rev. B* **80**, 165316 (2009).
  - [18] H.-M. Guo, G. Rosenberg, G. Refael, and M. Franz, *Phys. Rev. Lett.* **105**, 216601 (2010).
  - [19] A. Altland, D. Bagrets, L. Fritz, A. Kamenev, and H. Schmiedt, *Phys. Rev. Lett.* **112**, 206602 (2014).
  - [20] I. Mondragon-Shem, T. L. Hughes, J. Song, and E. Prodan, *Phys. Rev. Lett.* **113**, 046802 (2014).
  - [21] P. Titum, N. H. Lindner, M. C. Rechtsman, and G. Refael, *Phys. Rev. Lett.* **114**, 056801 (2015).
  - [22] B. Wu, J. Song, J. Zhou, and H. Jiang, *Chinese Physics B* **25**, 117311 (2016).
  - [23] P. V. Sriluckshmy, K. Saha, and R. Moessner, *Phys. Rev. B* **97**, 024204 (2018).
  - [24] J.-H. Zheng, T. Qin, and W. Hofstetter, *Phys. Rev. B* **99**, 125138 (2019).
  - [25] Y. Kuno, *Phys. Rev. B* **100**, 054108 (2019).
  - [26] R. Chen, D.-H. Xu, and B. Zhou, *Phys. Rev. B* **100**, 115311 (2019).
  - [27] X. S. Wang, A. Brataas, and R. E. Troncoso, *Phys. Rev. Lett.* **125**, 217202 (2020).
  - [28] C.-A. Li, B. Fu, Z.-A. Hu, J. Li, and S.-Q. Shen, *Phys. Rev. Lett.* **125**, 166801 (2020).

- [29] Y.-B. Yang, K. Li, L.-M. Duan, and Y. Xu, *Phys. Rev. B* **103**, 085408 (2021).
- [30] S. Velury, B. Bradlyn, and T. L. Hughes, *Phys. Rev. B* **103**, 024205 (2021).
- [31] D.-W. Zhang, L.-Z. Tang, L.-J. Lang, H. Yan, and S.-L. Zhu, *Sci. China-Phys. Mech. Astron.* **63**, 267062 (2020).
- [32] X.-W. Luo and C. Zhang, *arXiv:1912.10652v1*.
- [33] H. Wu and J.-H. An, *Phys. Rev. B* **102**, 041119 (2020).
- [34] L.-Z. Tang, L.-F. Zhang, G.-Q. Zhang, and D.-W. Zhang, *Phys. Rev. A* **101**, 063612 (2020).
- [35] H. Liu, Z. Su, Z.-Q. Zhang, and H. Jiang, *Chinese Physics B* **29**, 050502 (2020).
- [36] Q. Lin, T. Li, L. Xiao, K. Wang, W. Yi, and P. Xue, (2021), *arXiv:2108.01097 [cond-mat.mes-hall]*.
- [37] J. Claes and T. L. Hughes, *Phys. Rev. B* **103**, L140201 (2021).
- [38] G.-Q. Zhang, L.-Z. Tang, L.-F. Zhang, D.-W. Zhang, and S.-L. Zhu, *Phys. Rev. B* **104**, L161118 (2021).
- [39] K. Li, J.-H. Wang, Y.-B. Yang, and Y. Xu, *arXiv* (2021), *arXiv:2104.14097 [cond-mat.dis-nn]*.
- [40] T.-C. Yi, S. Hu, E. V. Castro, and R. Mondaini, *Phys. Rev. B* **104**, 195117 (2021).
- [41] E. J. Meier, F. A. An, A. Dauphin, M. Maffei, P. Massignan, T. L. Hughes, and B. Gadway, *Science* **362**, 929 (2018).
- [42] S. Stützer, Y. Plotnik, Y. Lumer, P. Titum, N. H. Lindner, M. Segev, M. C. Rechtsman, and A. Szameit, *Nature* **560**, 461 (2018).
- [43] G.-G. Liu, Y. Yang, X. Ren, H. Xue, X. Lin, Y.-H. Hu, H.-x. Sun, B. Peng, P. Zhou, Y. Chong, and B. Zhang, *Phys. Rev. Lett.* **125**, 133603 (2020).
- [44] F. Zangeneh-Nejad and R. Fleury, *Advanced Materials* **32**, 2001034 (2020).
- [45] W. Zhang, D. Zou, Q. Pei, W. He, J. Bao, H. Sun, and X. Zhang, *Phys. Rev. Lett.* **126**, 146802 (2021).
- [46] W. P. Su, J. R. Schrieffer, and A. J. Heeger, *Phys. Rev. Lett.* **42**, 1698 (1979).
- [47] P. G. Harper, *Proc. Phys. Soc. London, Sect. A* **68**, 874 (1955).
- [48] S. Aubry and G. André, *Phys. Soc.* **3**, 133 (1980).
- [49] D. J. Thouless, *Phys. Rev. B* **28**, 4272 (1983).
- [50] G. Roati, C. D'Errico, L. Fallani, M. Fattori, C. Fort, M. Zaccanti, G. Modugno, M. Modugno, and M. Inguscio, *Nature* **453**, 895 (2008).
- [51] H. P. Lüschen, S. Scherg, T. Kohlert, M. Schreiber, P. Bordia, X. Li, S. Das Sarma, and I. Bloch, *Phys. Rev. Lett.* **120**, 160404 (2018).
- [52] Y. Lahini, R. Pugatch, F. Pozzi, M. Sorel, R. Morandotti, N. Davidson, and Y. Silberberg, *Phys. Rev. Lett.* **103**, 013901 (2009).
- [53] Y. E. Kraus and O. Zilberberg, *Phys. Rev. Lett.* **109**, 116404 (2012).
- [54] S. Iyer, V. Oganessian, G. Refael, and D. A. Huse, *Phys. Rev. B* **87**, 134202 (2013).
- [55] M. Verbin, O. Zilberberg, Y. E. Kraus, Y. Lahini, and Y. Silberberg, *Phys. Rev. Lett.* **110**, 076403 (2013).
- [56] K. A. Madsen, E. J. Bergholtz, and P. W. Brouwer, *Phys. Rev. B* **88**, 125118 (2013).
- [57] L.-J. Lang, X. Cai, and S. Chen, *Phys. Rev. Lett.* **108**, 220401 (2012).
- [58] S. Ganeshan, K. Sun, and S. Das Sarma, *Phys. Rev. Lett.* **110**, 180403 (2013).
- [59] I. I. Satija and G. G. Naumis, *Phys. Rev. B* **88**, 054204 (2013).
- [60] Y. E. Kraus, Y. Lahini, Z. Ringel, M. Verbin, and O. Zilberberg, *Phys. Rev. Lett.* **109**, 106402 (2012).
- [61] M. Tezuka and N. Kawakami, *Phys. Rev. B* **85**, 140508 (2012).
- [62] W. DeGottardi, D. Sen, and S. Vishveshwara, *Phys. Rev. Lett.* **110**, 146404 (2013).
- [63] H. Jiang, L.-J. Lang, C. Yang, S.-L. Zhu, and S. Chen, *Phys. Rev. B* **100**, 054301 (2019).
- [64] T. Liu, H. Guo, Y. Pu, and S. Longhi, *Phys. Rev. B* **102**, 024205 (2020).
- [65] L.-J. Zhai, S. Yin, and G.-Y. Huang, *Phys. Rev. B* **102**, 064206 (2020).
- [66] T. Liu and X. Xia, *Phys. Rev. B* **104**, 134202 (2021).
- [67] T. Xiao, D. Xie, Z. Dong, T. Chen, W. Yi, and B. Yan, *Science Bulletin* **66**, 2175 (2021).
- [68] S. Nakajima, N. Takei, K. Sakuma, Y. Kuno, P. Marra, and Y. Takahashi, *Nature Physics* **17**, 844 (2021).
- [69] Y. Liu, X.-P. Jiang, J. Cao, and S. Chen, *Phys. Rev. B* **101**, 174205 (2020).
- [70] C. M. Dai, W. Wang, and X. X. Yi, *Phys. Rev. A* **98**, 013635 (2018).
- [71] S. Roy, T. Mishra, B. Tanatar, and S. Basu, *Phys. Rev. Lett.* **126**, 106803 (2021).
- [72] Y.-T. Hsu, X. Li, D.-L. Deng, and S. Das Sarma, *Phys. Rev. Lett.* **121**, 245701 (2018).
- [73] S. Xu, X. Li, Y.-T. Hsu, B. Swingle, and S. Das Sarma, *Phys. Rev. Research* **1**, 032039 (2019).
- [74] X. Li, J. H. Pixley, D.-L. Deng, S. Ganeshan, and S. Das Sarma, *Phys. Rev. B* **93**, 184204 (2016).
- [75] I. Chang, K. Ikezawa, and M. Kohmoto, *Phys. Rev. B* **55**, 12971 (1997).
- [76] F. Liu, S. Ghosh, and Y. D. Chong, *Phys. Rev. B* **91**, 014108 (2015).
- [77] Y. Wang, C. Cheng, X.-J. Liu, and D. Yu, *Phys. Rev. Lett.* **126**, 080602 (2021).
- [78] Y. Wang, L. Zhang, S. Niu, D. Yu, and X.-J. Liu, *Phys. Rev. Lett.* **125**, 073204 (2020).
- [79] L.-Z. Tang, G.-Q. Zhang, L.-F. Zhang, and D.-W. Zhang, *Phys. Rev. A* **103**, 033325 (2021).
- [80] R. El-Ganainy, K. G. Makris, M. Khajavikhan, Z. H. Musslimani, S. Rotter, and D. N. Christodoulides, *Nat. Phys.* **14**, 11 (2018).
- [81] Y. Ashida, Z. Gong, and M. Ueda, *Advances in Physics* **69**, 249 (2020).
- [82] E. J. Bergholtz, J. C. Budich, and F. K. Kunst, *Rev. Mod. Phys.* **93**, 015005 (2021).
- [83] Z. Gong, Y. Ashida, K. Kawabata, K. Takasan, S. Higashikawa, and M. Ueda, *Phys. Rev. X* **8**, 031079 (2018).
- [84] T. E. Lee, *Phys. Rev. Lett.* **116**, 133903 (2016).
- [85] S. Yao and Z. Wang, *Phys. Rev. Lett.* **121**, 086803 (2018).
- [86] F. K. Kunst, E. Edvardsson, J. C. Budich, and E. J. Bergholtz, *Phys. Rev. Lett.* **121**, 026808 (2018).
- [87] K. Zhang, Z. Yang, and C. Fang, *Phys. Rev. Lett.* **125**, 126402 (2020).
- [88] Z. Yang, K. Zhang, C. Fang, and J. Hu, *Phys. Rev. Lett.* **125**, 226402 (2020).
- [89] N. Okuma, K. Kawabata, K. Shiozaki, and M. Sato, *Phys. Rev. Lett.* **124**, 086801 (2020).
- [90] D. S. Borgnia, A. J. Kruchkov, and R.-J. Slager, *Phys. Rev. Lett.* **124**, 056802 (2020).
- [91] N. Hatano and D. R. Nelson, *Phys. Rev. Lett.* **77**, 570 (1996).

- [92] N. Hatano and D. R. Nelson, [Phys. Rev. B \*\*56\*\*, 8651 \(1997\)](#).
- [93] Q.-B. Zeng and Y. Xu, [Phys. Rev. Research \*\*2\*\*, 033052 \(2020\)](#).
- [94] X. Cai, [Phys. Rev. B \*\*103\*\*, 014201 \(2021\)](#).
- [95] S. Longhi, [Phys. Rev. B \*\*100\*\*, 125157 \(2019\)](#).
- [96] L. Zhou and W. Han, [Chin. Phys. B \*\*30\*\*, 100308 \(2021\)](#).
- [97] S. Longhi, [Phys. Rev. Lett. \*\*122\*\*, 237601 \(2019\)](#).
- [98] C. Wu, J. Fan, G. Chen, and S. Jia, [New Journal of Physics \*\*23\*\*, 123048 \(2021\)](#).
- [99] Y. Fu, J. H. Wilson, and J. H. Pixley, [Phys. Rev. B \*\*104\*\*, L041106 \(2021\)](#).
- [100] S. Longhi, [Phys. Rev. Lett. \*\*122\*\*, 237601 \(2019\)](#).
- [101] F. Song, S. Yao, and Z. Wang, [Phys. Rev. Lett. \*\*123\*\*, 246801 \(2019\)](#).
- [102] Z. Lu, Z. Xu, and Y. Zhang, [arXiv:2201.00488](#).